

10-1-1973

# Remote Wind Profile Measurement at Optical Frequencies Using a Spectral Density Approach

John E. Nuwer

*University of Texas at El Paso*

Jack Smith

*University of Texas at El Paso*

Fred J. Taylor

*University of Texas at El Paso*

Thomas H. Pries

*White Sands Missile Range, New Mexico*

Follow this and additional works at: [http://docs.lib.purdue.edu/lars\\_symp](http://docs.lib.purdue.edu/lars_symp)

---

Nuwer, John E.; Smith, Jack; Taylor, Fred J.; and Pries, Thomas H., "Remote Wind Profile Measurement at Optical Frequencies Using a Spectral Density Approach" (1973). *LARS Symposia*. Paper 24.

[http://docs.lib.purdue.edu/lars\\_symp/24](http://docs.lib.purdue.edu/lars_symp/24)

This document has been made available through Purdue e-Pubs, a service of the Purdue University Libraries. Please contact [epubs@purdue.edu](mailto:epubs@purdue.edu) for additional information.

**Conference on**  
**Machine Processing of**  
**Remotely Sensed Data**

**October 16 - 18, 1973**

The Laboratory for Applications of  
Remote Sensing

Purdue University  
West Lafayette  
Indiana

Copyright © 1973  
Purdue Research Foundation

This paper is provided for personal educational use only,  
under permission from Purdue Research Foundation.

REMOTE WIND PROFILE MEASUREMENT AT OPTICAL FREQUENCIES USING  
A SPECTRAL DENSITY APPROACH

John E. Nuwer, Jack Smith, Fred J. Taylor, and  
Thomas H. Pries\*

Department of Electrical Engineering  
The University of Texas at El Paso  
El Paso, Texas;  
\*Atmospheric Sciences Laboratory,  
White Sands Missile Range, New Mexico

I. ABSTRACT

The spectral properties of the intensity of a light beam, propagated in a turbulent atmosphere in the presence of wind shears, are studied. The theory of light propagation in a turbulent media is presented. Special attention is given to developing the theoretical characteristics of a spherical wave. These theoretical relations are numerically analyzed. The analysis indicate that the problem of remotely measuring winds can be automated. Several machine techniques are offered to accomplish this task.

II. INTRODUCTION

Atmospheric turbulence due primarily to wind shear and convective heating of the ground, has a noticeable effect on light propagation. This turbulence, characterized by small, random changes in the index of refraction along a propagation path, induces variations in the phase of electromagnetic waves passing through it. The phase variations induced can result in amplitude variations of the wave. The energy in a light beam is redistributed in passing through turbulence in such a way that it exhibits intensity fluctuations known as scintillations, i.e., an optical wave with uniform intensity across a wavefront, upon travelling through a turbulent atmosphere, will have bright and dark "spots" across a wavefront. At any instant, the random scintillation pattern observed in a plane parallel to the wavefront will contain information about the spatial Fourier components of the turbulence. The most effective scale size producing the intensity variations is determined by,  $\sqrt{\lambda L}$ , where  $\lambda$  is the wavelength and L is the path length. The wind across a propagation path will move the turbulent eddies in the atmosphere through the light beam, thus moving the "spots" in the scintillation pattern across a fixed observation point at a rate proportional to the wind velocity. The temporal frequency of the intensity variations at a fixed observation point, therefore, depends on the transverse component of the wind along the path. The predominate frequency is proportional to the mean wind speed divided by the Fresnel-zone size.

Since atmospheric turbulence induces amplitude and phase changes in an electromagnetic wave, the question to be considered is whether these changes can be used to measure the atmospheric effects which produced them. Scintillation drift at radio frequencies has been used for years to measure ionospheric winds (Mitra, 1949). This is possible since the motion of scintillation patterns is directly related to winds across the propagation path. Two methods suggest themselves for measuring atmospheric winds by using optical frequency radiation: the use of two sensors in the scintillation pattern so that the transition time of light and dark spots may be measured and related to the wind velocity, or the use of one sensor in the pattern to determine the temporal frequency of the intensity variations. When the motion of turbulent eddies is considered the spatial covariance function of the intensity variations can be used to determine the temporal Fourier components. The covariance function for the plane wave case is useful in measuring ionospheric winds. For line-of-sight propagation near the earth's surface, the covariance for the spherical wave case as developed by Schmeltzer (1967) is more appropriate. In order to actually measure the wind velocity profile using the formulations of Tatarski (1961), Schmeltzer (1967), or

Lee and Harp (1969) the integral equation for covariance must be inverted. Peskoff (1968) developed an analytical solution for the equation for the plane wave case by performing the inversion and demonstrated the feasibility of sensing wind profiles. Shen (1970), using the correlation and slope-at-zero-lag of the spherical wave covariance function, developed a numerical inversion and using microwaves he concluded that winds could be remotely sensed using such a method. Predominate in the actual measurement of winds at optical frequencies have been Lawrence, Ochs, and Clifford (1972). They have successfully constructed and tested an instrument which measures the mean cross-wind component over a path in a real time. Their method is based on the slope of the spherical-wave covariance function at zero delay, as opposed to the delay-time-to-peak approach of Morgan and Bowles (1968).

This paper will deal with the extraction of significant characteristics of the wind along a propagation path using the temporal-power spectra and pattern recognition techniques.

### III. THEORY

Consider a spherical optical wave with wavenumber  $k$ , propagating in the  $z$ -direction to a receiver plane at  $z=L$ . The temporal-power spectrum of the log-amplitude of the intensity variations is (Clifford, 1971)

$$W(f) = 16\pi^2 k^2 \int_0^L dz \int_{\frac{2\pi f}{v}}^{\infty} dK K \phi(K) [(Kv)^2 - (2\pi f)^2]^{-1/2} \sin^2 \left[ k^2 \frac{z(L-z)}{2kL} \right]. \quad (1)$$

$K$  is the spatial wavenumber interpreted as  $K = 2\pi/\ell$  where  $\ell$  is the scale size of turbulence and  $v$ , a function of  $z$ , is the wind profile along the path.

The form of  $\phi(K)$  the refractivity spectrum, and its effective limits are necessary for this formulation. Energy is introduced by convection caused by the heating of the ground and wind shear. Turbulent energy, then, is introduced by the action of scale sizes larger than some minimum value  $L_0$ , called the outer scale of turbulence, corresponding to a wavenumber  $K_0 = 2\pi/L_0$ . Near the ground  $L_0$  is assumed to be on the order of the height above ground. For spatial wavenumbers larger than  $K_0$ , the scale size is smaller than the distance from the ground and assumptions of homogeneity and isotropy are more nearly correct. Kolmogorov (1961) proposed a  $K^{-11/3}$  dependence of the spectrum for wavenumbers greater than  $K_0$ ; this type of dependence has also been indicated by experiment. Energy from larger eddies, as they break apart, is transferred down to smaller scales until a scale size  $\ell_0$  is reached where the energy is dissipated as heat, this is called the inner scale of turbulence. In the range of scale sizes between  $L_0$  and  $\ell_0$ , called the inertial subrange, the refractive-index spectrum has been assumed, following Tatarski (1961) to have the form

$$\phi(K) = 0.033 C_n^2 K^{-11/3} \exp(-K^2/K_m^2) \quad (2)$$

under the condition  $K_m \ell_0 = 5.92$ . The equation is a poor approximation for  $K < K_0$ ; the equation is a reasonable approximation for  $K > K_m$ .  $C_n^2$ , the refractive index structure coefficient is a measure of the intensity of the refractive-index fluctuations. Substantial uncertainty exists about the mean and variance of  $C_n^2$  under specific meteorological situations.

### IV. CALCULATIONS

The theoretical expression for the temporal frequency of a spherical wave is given by Eq. (1). For numerical simulation it is the shape of the spectral densities which is of interest. Therefore, the constant leading terms of  $W(f)$  are ignored. The spectral density  $\phi(K)$  is assumed to have the  $K^{-11/3}$  dependence proposed by Kolmogorov.  $C_n^2(z)$  is assumed to be constant over the path and its variations are neglected. An alternate approach by Lawrence, Ochs, and Clifford (1972) is to make  $C_n^2(z)$  piecewise constant over the path. In order to calculate the frequency spectra  $W(f)$  is assumed to have the form

$$W(f) = \int_0^L dz \int_{\frac{2\pi f}{v}}^{2000\pi} dK K^{-8/3} f_1(K, v; z) f_2(K, z) \quad (3)$$

where  $f_1(K, v; z)$  is the square root dependence on  $K$  and  $v$ , the dependence on  $z$  through  $v(z)$  is implicit, and  $f_2(K, z)$  is the path weighting function. Recall that  $f_1(K, v; z)$  is of the form

$$f_1(K, v; z) = [(Kv)^2 - (2\pi f)^2]^{-1/2} \quad (4)$$

and

$$f_2(K, z) = \sin^2 \left[ K^2 \frac{z(L-z)}{2kL} \right]. \quad (5)$$

The upper limit of integration in Eq. (3) results from the fact that scale sizes smaller than  $1 \text{ mm}$  are not expected in real meteorological situations.

To evaluate Eq. (3) a two-dimensional routine was not available so two one-dimensional integrations were used. A Simpson's rule integration was employed which performed successive interval halving until desired accuracy was obtained or a specified number of halvings were executed. A limit on the number of halvings was necessary to keep run time acceptable. If the desired accuracy was not obtained a diagnostic was printed. The integration over  $K$  was performed first and then the integration over  $z$ . Due to the large range of  $K$  and the "roughness" of the integrand, it was necessary to subdivide the integration into ten smaller divisions. Each division was again subdivided into ten additional subdivisions. In order to minimize run time, if the sum of the integrations over ten subdivisions was within a prespecified error tolerance the integration was accepted, otherwise the interval was re-subdivided. In the program run, three place accuracy was required of the integration with ten halvings allowed. The tolerance on the subdivisions of the  $K$  integration was one-hundredth.

Another problem arises in the  $K$  integration at its lower limit. When  $K=2\pi f/v$  the  $f_1(K, v; z)$  function approaches infinity. This difficulty was overcome by allowing the lower limit on  $K$  to be  $(2\pi f/v) + \epsilon$ , integrating, and then adding to the result an approximation of the area missed. Let  $K=(2\pi f/v) + \epsilon$ , and consider the integrand

$$K^{-8/3} f_1(K, v; z) f_2(K, z) = \left( \frac{2\pi f}{v} + \epsilon \right)^{-8/3} \left[ \left( \frac{2\pi f}{v} + \epsilon \right)^2 v^2 - (2\pi f)^2 \right]^{-1/2} \sin^2 \left[ \left( \frac{2\pi f}{v} + \epsilon \right)^2 C \right] \quad (6)$$

where  $C=z(L-z)/2kL$ . For  $\epsilon$  very small it may be neglected in all but the  $f_1(K, v; z)$  term; expanding

$$K^{-8/3} f_1(K, v; z) f_2(K, z) \sim \left( \frac{2\pi f}{v} \right)^{-8/3} [\epsilon v (4\pi f + \epsilon v)]^{-1/2} \sin^2 \left[ \left( \frac{2\pi f}{v} \right)^2 C \right]. \quad (7)$$

The integration over  $K$  from  $2\pi f/v$  to  $(2\pi f/v) + \epsilon$  then becomes, neglecting second order terms,

$$\int_0^\epsilon d\epsilon K^{-8/3} f_1(K, v; z) f_2(K, z) \sim \left( \frac{2\pi f}{v} \right)^{-8/3} \sin^2 \left[ \left( \frac{2\pi f}{v} \right)^2 C \right] \int_0^\epsilon d\epsilon (4\pi f \epsilon)^{-1/2} \sim \left( \frac{2\pi f}{v} \right)^{-8/3} \sin^2 \left[ \left( \frac{2\pi f}{v} \right)^2 z \frac{(L-z)}{2kL} \right] \left( \frac{\epsilon}{\pi f v} \right)^{1/2}. \quad (8)$$

This result is then added to the value of the integral over the range  $(2\pi f/v) + \epsilon$  to  $2000\pi$ . For the program run  $\epsilon$  was set to be one-thousandth.

## V. RESULTS

Using the program developed to compute the log-amplitude spectral density, plots were obtained for various wind profiles. In all cases the magnitudes have been scaled for convenience by the maximum of the spectral density for a constant  $1 \text{ m/s}$  wind. The important consideration is the relative shape of the spectral density and how it varies for different wind profiles, not the absolute magnitude.

Several scaling ideas are important in estimating the characteristic frequencies associated with the shape of the spectra under different wind conditions and for different path lengths. A slightly modified form of Eq. (1) is given by Eq. (9).

$$W(f) = 16\pi^2 k^2 \int_0^L dz \int_0^\infty \frac{\phi[(K'^2 + \omega^2/v^2)^{1/2}]}{v} \sin^2 \left[ \frac{(K'^2 + \omega^2/v^2)z(L-z)}{2kL} \right] dk' \quad (9)$$

where  $K'^2 = K^2 - \omega^2/v^2$  and  $\omega = 2\pi f$ .

Eq. (9) shows that except for a magnitude scaling by  $1/v$  the result of the integration over  $K'$  is dependent on  $2\pi f/v$ . This fact implies that the 1 m/s wind profiles can be used to determine spectra for other wind velocities. For example the spectral density associated with 10 m/s cross-wind could be obtained from the 1 m/s spectrum by multiplying the frequency scale by 10, and dividing all magnitudes by the same factor.

The spectral densities of five constant winds from 1 m/s to 5 m/s have been compared with the result that the direct linear relationship between the spectral densities, which appears in the theory, was reproduced by the numerical calculation. If, for a wind of  $v$  m/s the amplitude of the spectral density at a frequency  $f$  is  $A(f)$ , then the amplitude of the spectral density of a wind which is a constant  $nv$  m/s at a frequency  $f_n = nf$  is  $A_n(f_n)$ . The following relationship has been found to be true

$$A_n(f_n) = \frac{A(f)}{n} \quad (10)$$

This linear relation is true to the accuracy of the calculations, 3 significant figures. In addition Eq. (10) is true for linear winds and winds which are triangular, quadratic, and sinusoidal if the winds are also scaled linearly. For example, if for a wind profile of the form

$$v = az + b \quad (11)$$

with a mean of  $v$  m/s, the profile of another wind is of the form

$$v = naz + nb \quad (12)$$

with a mean of  $nv$  m/s, then Eq. (10) holds. These relations have also been verified for the plane wave case.

The shape of the spectral density for different path lengths can be determined by considering that, for a given frequency, the magnitude of the components is determined by integrating  $K$  from  $\omega/v$  to infinity. See Eq. (1). Scale size can be expressed in terms of Fresnel zone size. For example

$$K = n\pi/\sqrt{\lambda L}.$$

Thus for a given  $\omega/v$  variations in path length scale the spectral frequencies by  $1/\sqrt{L}$ .

The implication is then that a set of universal spectral densities based on a profile set with a mean of 1 m/s may be calculated and the results extrapolated for the case of any wind with a given mean.

Calculations for the path weighting function

$$f_2(K, z) = \sin^2 \left[ K^2 \frac{z(L-z)}{2kL} \right] \quad (13)$$

are shown in Figs. 1 and 2. These figures show  $f_2(K, z)$  for two constant  $K$ 's based on a 1 km path. A rough idea of the general shape of the respective weighting functions is obtained from these figures and consideration of Eq. (13). The sinusoidal nature of the equations is distorted in the figures because all maxima and minima are not plotted. The spatial weighting function negligibly weights points near the ends of the path, always weights to some extent the center of the path, and weights most those points slightly off the center of the path. Note that the spatial weighting function is symmetric about the center of the path. It can be shown that the plane wave case is asymmetric and weights most heavily points near the transmitter end of the path, negligibly weights points near the receiver end of the path, and weights to some extent those points near the center and slightly toward the transmitter from the center of the path.

Figure 3 is a plot of the spectral density for a constant 1 m/s wind and a path length of 1 kilometer. The spectral densities are individually scaled. Three regions are evident in the spectral density: the first is a fairly constant, higher energy, region at low frequencies; the second a transition region in which the energy drops off rather smoothly with increasing frequency; and the third a lower energy region where the energy drops off very slowly with increasing frequency. These three regions are evident in all the spectral densities calculated. The abrupt dips in several of the spectral densities plotted are due to truncation and computational error and not to be expected in real situations.

The effects of a varying wind profile on the spectral density are shown in Fig. 4. The basic wind profile is a constant 1 m/s wind; to this has been added a pulse of 2 m/s of width  $L/5$  which is centered at  $L/10$ ,  $3L/10$ ,  $L/2$ ,  $7L/10$ , and  $9L/10$  for five different cases. The effects of the spatial weighting functions mentioned above are obvious. Note that the symmetry of the weighting function implies that moving the pulse to positions symmetric with respect to the center of the path has the same effect whether it is on the transmitter or receiver side. The abrupt changes in some of the spectral densities are due to the discontinuity in the wind profile which is not realistic. This center symmetry is not present in cases of plane wave spectra. Consider how the spectral density for a 1 m/s constant wind will change for a uniform shear about a mean of 1 m/s wind. Assume a wind profile which linearly increases from  $1/2$  m/s at the transmitter to  $3/2$  m/s at the receiver. The profile weighting function will be a minimum at the transmitter and increases to a maximum at the center of the path. Since the ends of the path have little weight and the profile weighting function will be very close to that for a 1 m/s constant wind near the center of the path, the spectral density will change little. Figure 5 demonstrates this. Again due to the symmetry of the spatial weighting function the spectral density for the shear profile is identical to that for a wind which decreases linearly from  $3/2$  m/s at the transmitter to  $1/2$  m/s at the receiver.

From the above it is apparent that the spectral density will change as a direct function of the wind profile and that information about the wind profile is intrinsic to the spectral density. Since wind profile information is contained in the spectral density, the problem becomes one of extracting the information quickly and efficiently in a real time environment. Figure 6, then, is a set of spectral densities for a profile set with a mean of 1 m/s. In all cases the spectral densities are determined by the wind profile and information on the wind profile may be determined from the spectral density.

In using the spherical wave case two difficulties are apparent from consideration of Fig. 5. The first is that for winds which have a uniform shear, the direction of the shear is not obtainable from the spectral density. The second difficulty is discrimination between a constant 1 m/s wind and one which has a uniform shear from  $3/4$  to  $5/4$  m/s. This distinction is not critical for this low wind speed, however, recall by the scaling property, Eq. (9), that this same type of distinction would have been made for a wind of 10 m/s mean with a uniform shear from 7.5 to 12.5 m/s. Both of these difficulties can be overcome through an accurate algorithm to distinguish different spectral densities and an additional wind measurement in the transmitter or receiver plane.

## VI. AUTOMATED WIND PROFILE MEASUREMENT

A machine to determine wind profiles from spectral density information would have four primary components. The first would be a measurement device consisting of the detector itself and an appropriate processor to extract the necessary measurements. This would consist of a photodiode or similar sensor with the necessary optics, and an electronic processor which would select a set of frequencies and make a measure of the spectral density at each frequency. A statistical analysis needs to be performed on the spectral densities to determine which measurements at which frequencies would contain the most information. The measurements could represent amplitudes, first and second order derivatives. A/D converters would digitize the data for processing. The second component of the profile recognizing machine would be a pattern recognition device which would predict the mean wind. This device must be a trainable pattern classifier since in a field environment the spectral densities of the wind profiles will be a function of the prevalent meteorological conditions. Following the mean recognizer would be a scaler, which would scale the data, using the scaling rules previously discussed, into a universal profile set such as Fig. (6). The output of the scaler would be fed to a pattern recognizer which would classify the data as belonging to a given profile. This would be the last component of the profile recognition machine. Fig. (7) is a block diagram of such a machine.

Both of the pattern recognition devices must be trainable for specific field environments. This implies the existence of a memory in which each mean and each profile to be recognized would be

stored. This memory would be an interchangeable device so that in practice a separate memory would be obtained for each field condition in which the profile recognizer is to be used. Then, in a given field situation, the appropriate memory would be connected to the device. Each memory would be trained for a specific field environment.

Consider how such a trainable pattern recognition device, where the memory is considered as part of the device, would be constructed. The measurement system would be set up in a field environment where it was desired to use the machine. Fig. (8) illustrates a typical training set up. When a profile which is desired to be identified appears along the path, the selector is activated and both the spectra measurements and the corresponding profile identifiers are stored in the memory. Suppose R such measurement sets are generated. Each of the spectra measurements will be a set of d measurements at d frequencies. These measurements may be visualized as a d-vector where each of the d-basis is a frequency at which a measurement is made and the coordinates are the respective measurements. For each profile there exists in the memory device, then, what is essentially a d-vector  $\bar{P}_i$ ,  $i=1, \dots, R$ .

Given these R d-vectors  $\bar{P}_i$ , a unique profile, is associated with each one. Note that the assumption has been made that each profile has the same mean: a similar procedure would be followed for the mean recognition device in conjunction with the scaler to generate the profile set. For an arbitrary input,  $\bar{X}$ , to the profile recognition machine the Euclidean distance between  $\bar{X}$  and  $\bar{P}_i$  is

$$|\bar{X} - \bar{P}_i| = \sqrt{(\bar{X} - \bar{P}_i) \cdot (\bar{X} - \bar{P}_i)}, \quad i=1, \dots, R. \quad (14)$$

A minimum distance classifier may be constructed which will associate  $\bar{X}$  with profile  $i_0$  if  $|\bar{X} - \bar{P}_{i_0}| < |\bar{X} - \bar{P}_i|$  for  $i=1, \dots, R$ ,  $i \neq i_0$ . Equivalently, the squared distance  $|\bar{X} - \bar{P}_i|^2$  may be compared. Squaring both sides of Eq. (14) yields

$$|\bar{X} - \bar{P}_i|^2 = (\bar{X} - \bar{P}_i) \cdot (\bar{X} - \bar{P}_i) = \bar{X} \cdot \bar{X} - 2\bar{X} \cdot \bar{P}_i + \bar{P}_i \cdot \bar{P}_i. \quad (15)$$

Since  $\bar{X} \cdot \bar{X}$  will be a constant for all  $i=1, \dots, R$  the selection may be affected by comparing  $\bar{X} \cdot \bar{P}_i - 1/2 \bar{P}_i \cdot \bar{P}_i$  and choosing the maximum. Discriminant functions

$$g_i(\bar{X}) = \bar{X} \cdot \bar{P}_i - \frac{1}{2} \bar{P}_i \cdot \bar{P}_i, \quad i=1, \dots, R \quad (16)$$

may then be created and the classification made by associating  $\bar{X}$  with whichever profile corresponds to the largest  $g_i(\bar{X})$ . Note that  $g_i(\bar{X})$  is a linear function. Letting the components of  $\bar{P}_i$  be  $P_{i1}, P_{i2}, \dots, P_{id}$  and the constant  $-1/2 \bar{P}_i \cdot \bar{P}_i$  be  $P_{i,d+1}$  then  $g_i(\bar{X})$  is

$$g_i(\bar{X}) = P_{i1}x_1 + P_{i2}x_2 + \dots + P_{id}x_d + P_{i,d+1}, \quad i=1, \dots, R \quad (17)$$

where the  $x_1, x_2, \dots, x_d$  are the components of  $\bar{X}$ . Assuming that an additional element  $P_{i,d+1} = -1/2 \bar{P}_i \cdot \bar{P}_i$  is added to each measurement set in the memory, then a linear machine may be built which will affect the profile classification as in Fig. (9). Recall that this memory is for the specific field environment in which the machine was trained. For each field environment to be considered another memory will have to be created.

Effective profile recognition can be accomplished using the above method. In any given situation in which the profile recognition machine is to be used, wind profiles could be recognized if an appropriately trained memory was available.

An alternative pattern selection procedure would rely on the statistics collected in the training procedure described previously. Assume that the patterns in each of the R categories are random variables governed by R distinct probability functions. Let  $p(\bar{X}/i)$  be the probability of occurrence of pattern  $\bar{X}$ , given that it belongs to category  $i$ , and that the  $p(\bar{X}/i)$  are known functions; they could be approximated from the statistics collected by computer processing of the data and statistical inference. The probability of each class,  $p(i)$ , could also be obtained. Statistical decision theory can then be used to establish discriminant functions for the different classes if a loss function,  $\lambda(i/j)$ , is defined for  $i=1, \dots, R$  and  $j=1, \dots, R$ . The loss function would be a measure of the cost incurred by misclassification. With the above functions specified an optimum, Bayes, machine can be constructed. A Bayes classifier in a simplified block diagram is given by Fig. (10).

In order to try and minimize the number of measurements made the generalized sequential probability ratio test (GSPRT) can be used (Mendel, 1970). After  $n$  measurements are made, the generalized sequential probability ratios for each pattern class are computed as

$$\mu_n(\bar{X}|i) = \frac{p_n(X|i)}{\left[ \prod_{k=1}^R p_n(X|k) \right]^{\frac{1}{R}}} \quad i=1, \dots, R, n=1, \dots, d \quad (18)$$

where  $p_n(\bar{X}|i)$  is the conditional probability density function of  $\bar{X}=(x_1, x_2, \dots, x_n)^T$  for pattern class  $i$ . The  $\mu_n(\bar{X}|i)$  is then compared with the stopping boundary,  $A(i)$ , of the  $i$ th pattern class. The decision rule is to reject pattern class  $i$  from consideration if

$$\mu_n(\bar{X}|i) < A(i) \quad i=1, \dots, R.$$

The stopping boundary is determined by

$$A(i) = \frac{1 - e_{ii}}{\left[ \prod_{k=1}^R (1 - e_{ik}) \right]^{\frac{1}{R}}} \quad i=1, \dots, R \quad (19)$$

where  $e_{ij}$  is the probability of classifying  $\bar{X}$  in class  $i$  when  $\bar{X}$  is actually in class  $j$ .

Fig. (11) is a block diagram of a sequential classifier. This type of classification assumes that the process will be terminated when  $n=d$  otherwise more features than can be tolerated may be required and the average number of feature measurements may be very large if the  $e_{ij}$ 's are very small. The procedure is to carry out the process until a decision  $\mu$  is reached or stage  $d$  is reached. If no decision is reached by stage  $d$  the pattern is classified as belonging to the class with the largest generalized sequential probability ratio.

#### BIBLIOGRAPHY

1. Clifford, S. F., "Temporal-Frequency Spectra for a Spherical Wave Propagating Through Atmospheric Turbulent," *J. Opt. Soc. Am.*, vol. 61, pp 1285-92, 1971.
2. Kolmogorov, A., in Turbulence, Classic Papers on Statistical Theory, S. K. Friedlander and L. Topper, Eds., New York: Interscience, p 151, 1961.
3. Lawrence, R. S., G. R. Ochs, and S. F. Clifford, "Use of Scintillations to Measure Average Wind Across a Light Beam," App. Opt., Vol. 11, #2, 1972.
4. Lee, R. W., and J. C. Harp, "Weak Scattering in Random Media, with Applications to Remote Probing," Proc. IEEE, Vol. 57, #4, pp 375-406, 1969.
5. Mendel, J. M. and K. S. Fu, Adaptive Learning and Pattern Recognition Systems, Academic Press, New York, 1970.
6. Mitra, S. N., Proc. IEEE, 96-111, 441, 1969.
7. Morgan, M. G., and K. L. Bowles, Science 161, 1139, 1949.
8. Peskoff, A., "Theory of Remote-Sensing of Clear Air Turbulence Profiles," J. Opt. Soc. Am., Vol. 58, pp 1032-40, 1968.
9. Schmeltzer, R. W., "Means, Variances, and Covariances for Laser Beam Propagation Through a Random Medium," Quart. Appl. Math., vol. 24, pp 339-54, 1967.
10. Shen, L., "Remote Probing of Atmosphere and Wind Velocity by Millimeter Waves," IEEE Trans. Ant. Prop., vol. 18, pp 493-7, 1970.
11. Tatarski, V. I., Wave Propagation in a Turbulent Medium, New York: McGraw-Hill, 1961.

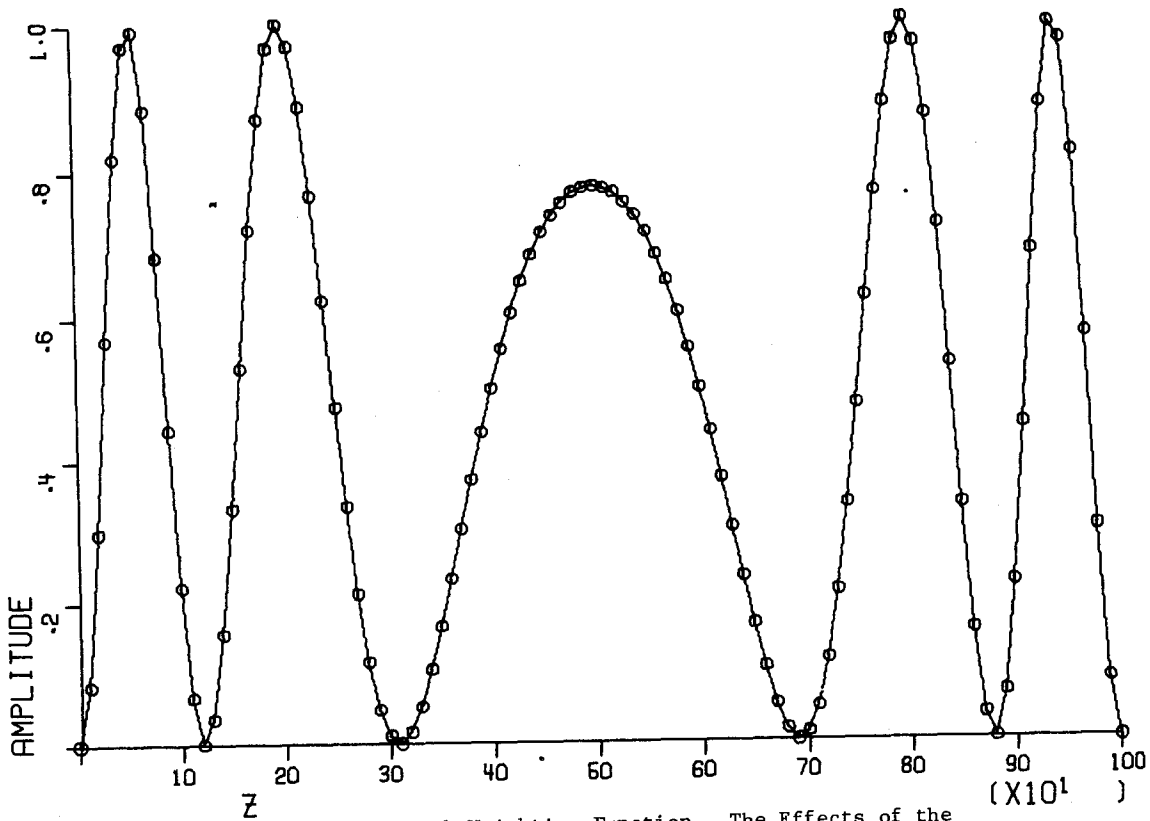


Figure 1. Path Weighting Function. The Effects of the Spatial Weighting Function, Sine Squared Term, for a Spherical Wave,  $K=500$ , and a Path Length of 1 km.

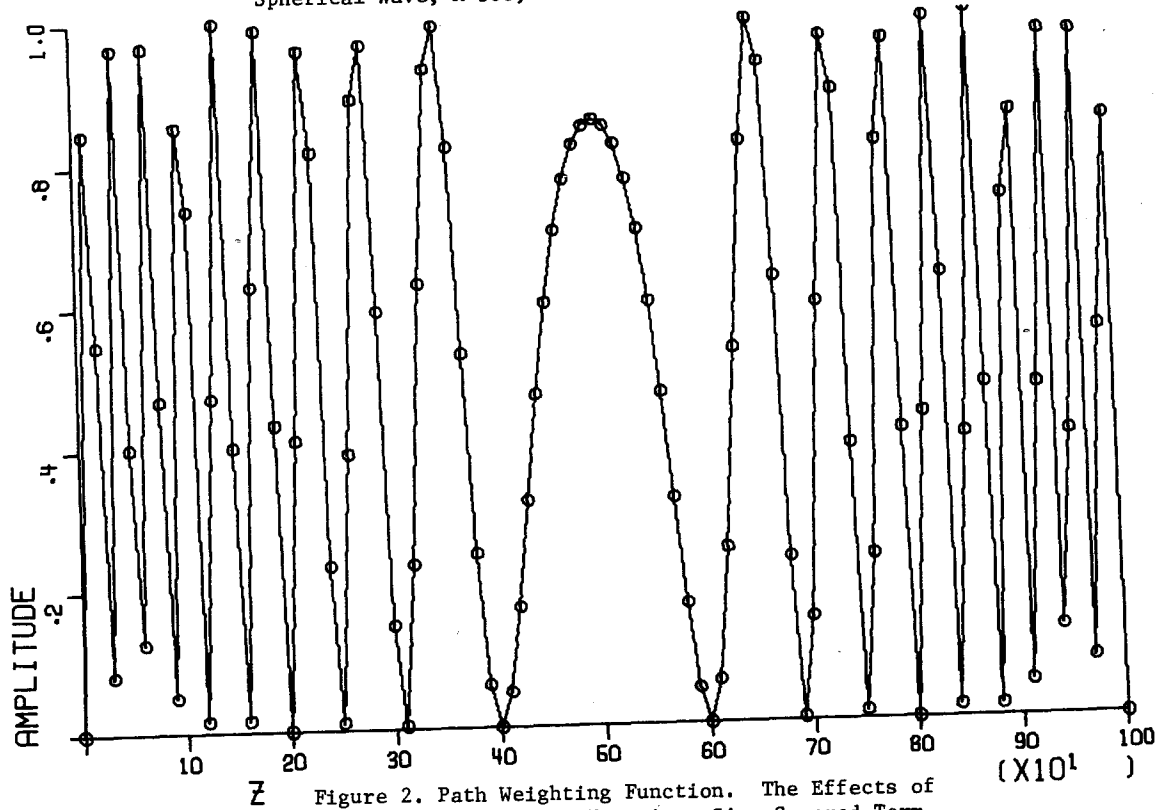


Figure 2. Path Weighting Function. The Effects of the Spatial Weighting Function, Sine Squared Term, for a Spherical Wave,  $K=250$ , and a Path Length of 1km.

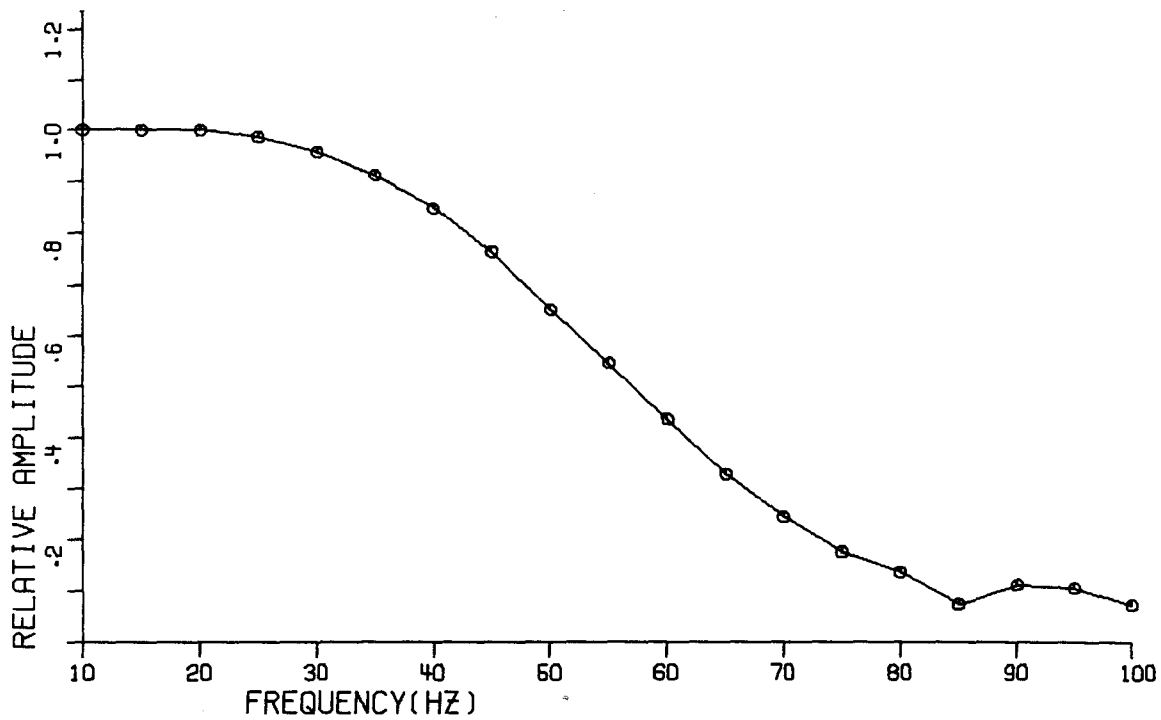


Figure 3. Temporal-Frequency Spectrum for a Spherical Wave, 1 m/s Constant Crosswind Over the Optical Path.

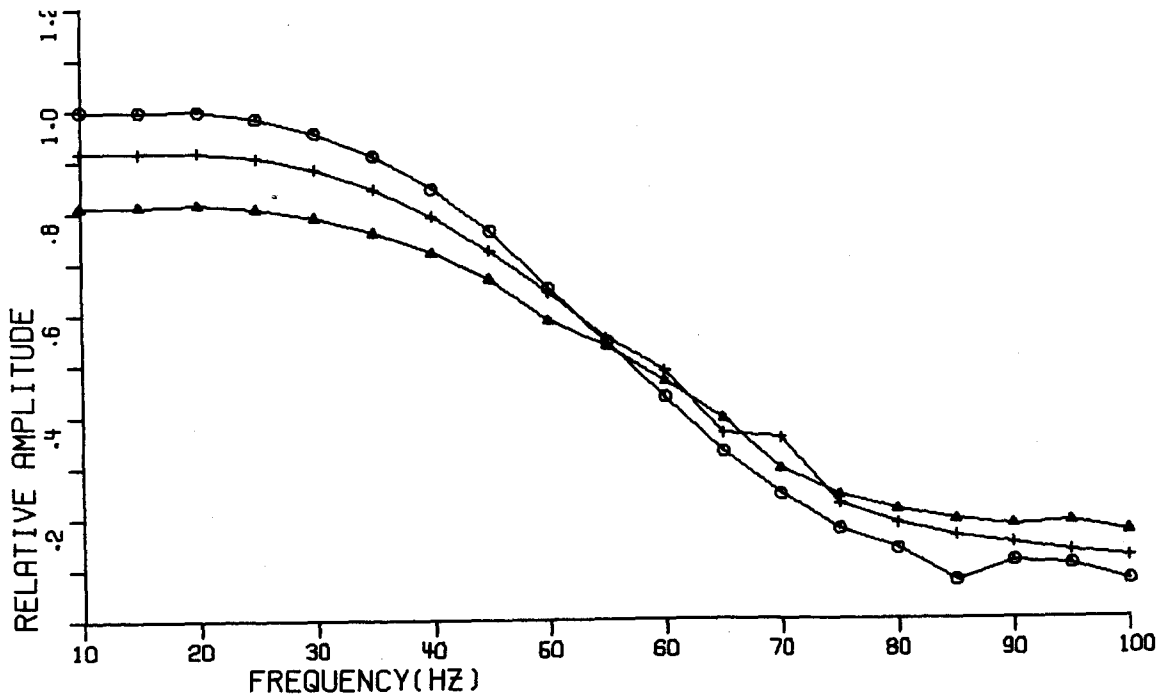


Figure 4. Variations in the Temporal-Frequency Spectrum of the 1 m/s Wind Caused By: a 2 m/s Pulse at L/10 or 9L/10, Circles, a 2 m/s Pulse at 3L/10 or 7L/10, Crosses, a 2 m/s pulse at L/2, Triangles.

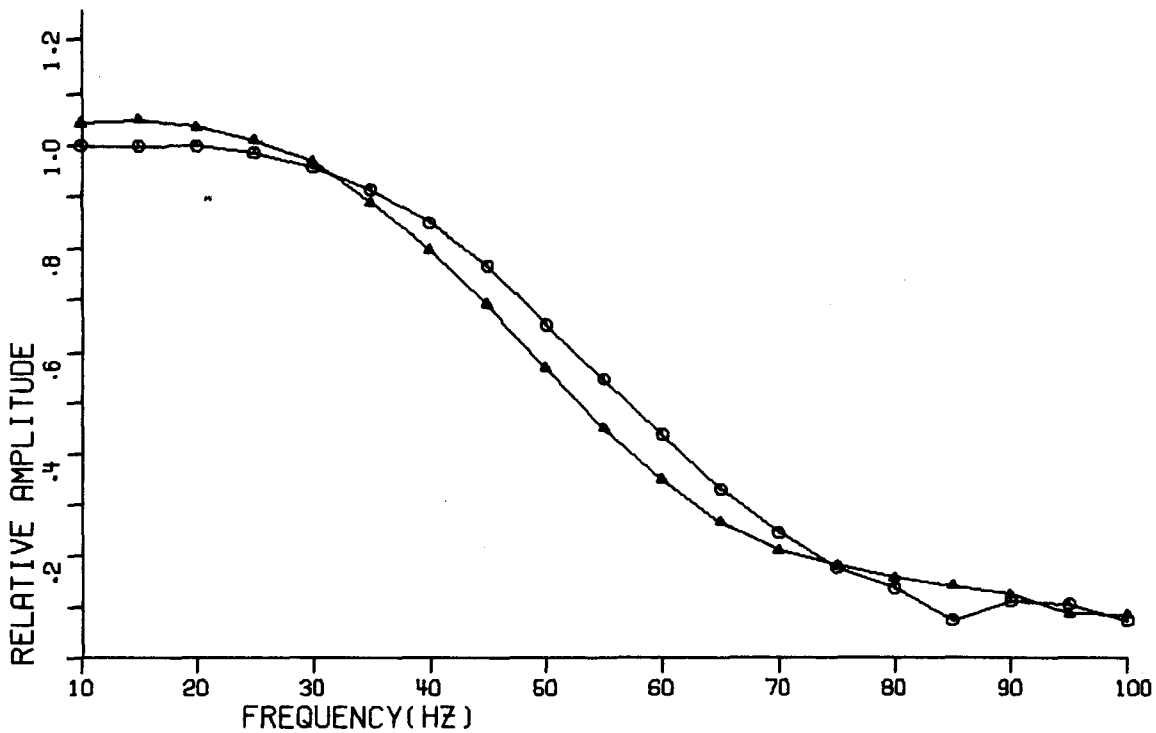


Figure 5. Variations In The Temporal-Frequency Spectrum Of The 1 m/s Wind Caused By A Uniform Shear. Constant 1 m/s , Circles, And The Triangles Represent The Spectrum For A Uniform Crosswind Variation From 1/2 m/s To 3/2 m/s Over The Optical Path.

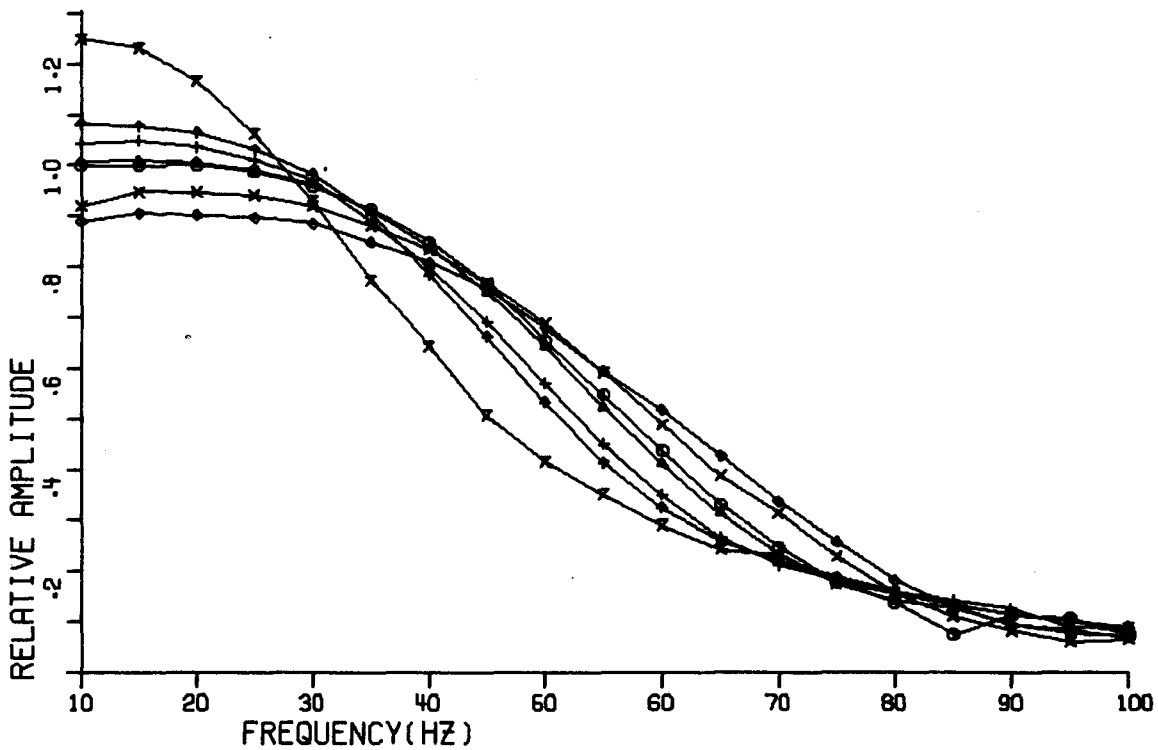


Figure 6. Spectral Profile Set For A Spherical Wave: 0 Constant 1 m/s:  $\Delta$  Uniform Shear 3/4 m/s To 5/4 m/s: + Uniform Shear 1/2 To 3/2 m/s: x Centered Triangular Shear 3/4 To 5/4 to 3/4 m/s:  $\diamond$  Centered Triangular Shear 1/2 To 3/2 To 1/2 m/s:  $\uparrow$  Centered Triangular Shear 5/4 To 3/4 To 5/4 m/s: x Centered Triangular Shear 3/2 To 1/2 To 3/2 m/s.

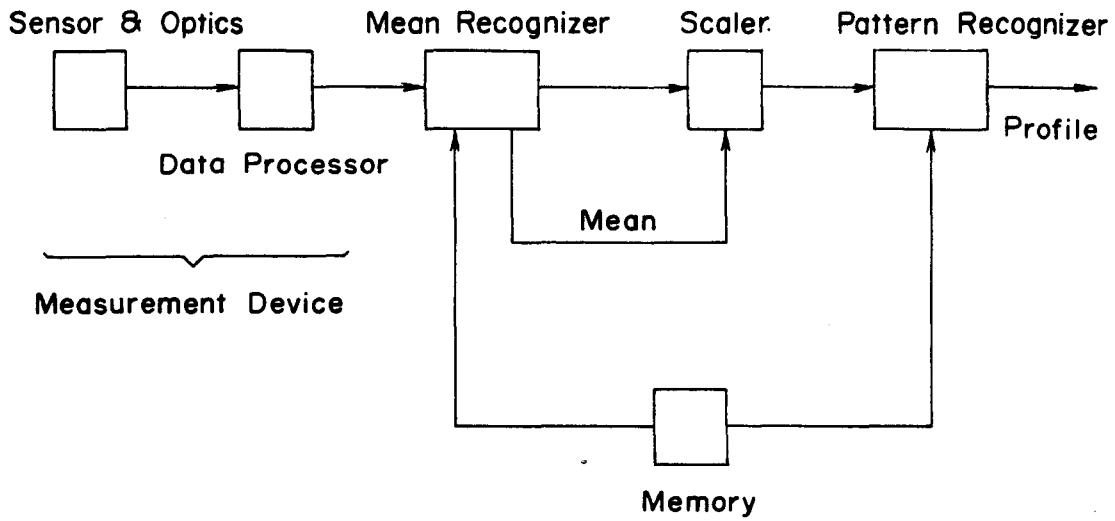


Figure 7. Spectral Profile Recognition Machine. Block Diagram

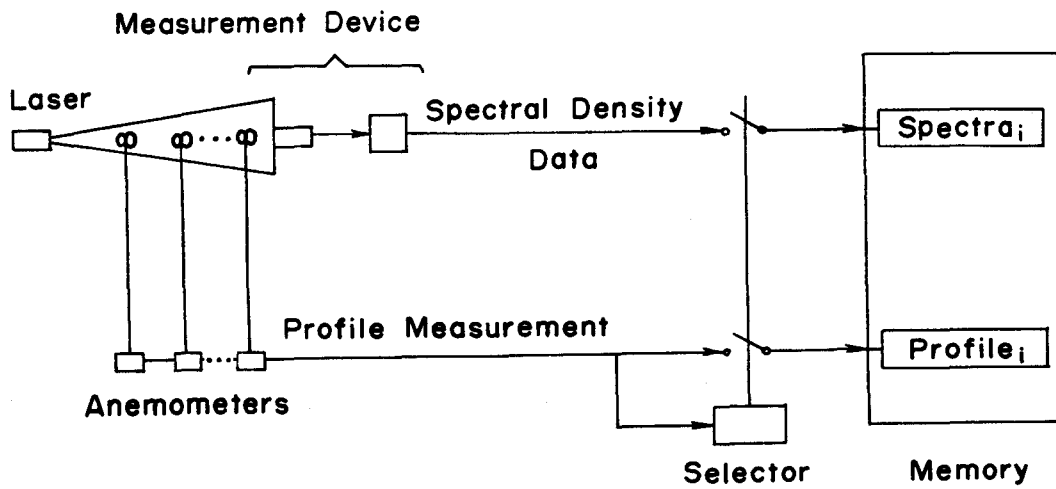


Figure 8. Trainable Spectral Profile Recognition Device And Technique

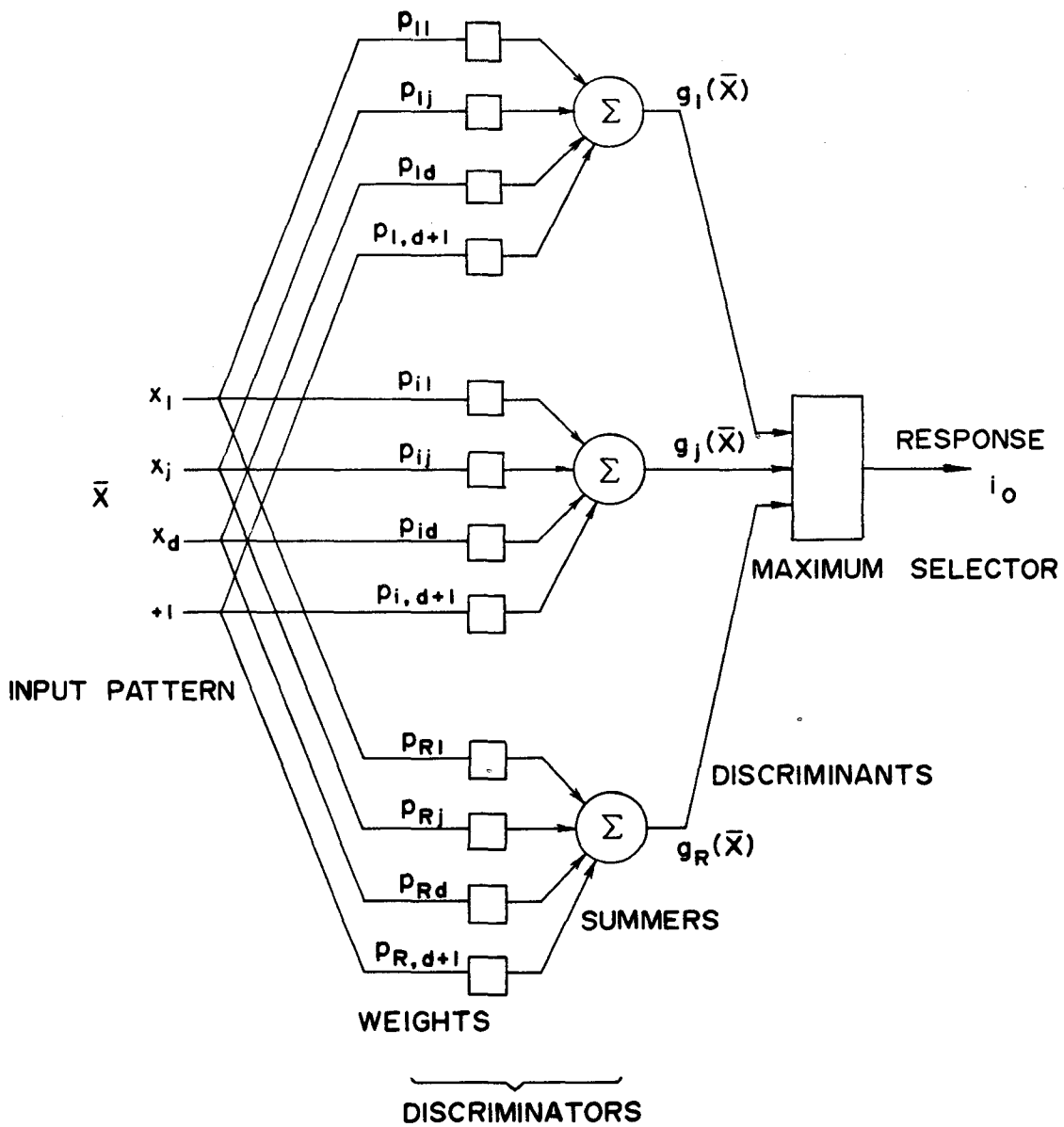


Figure 9. Linear Pattern Recognition Device. Block Diagram

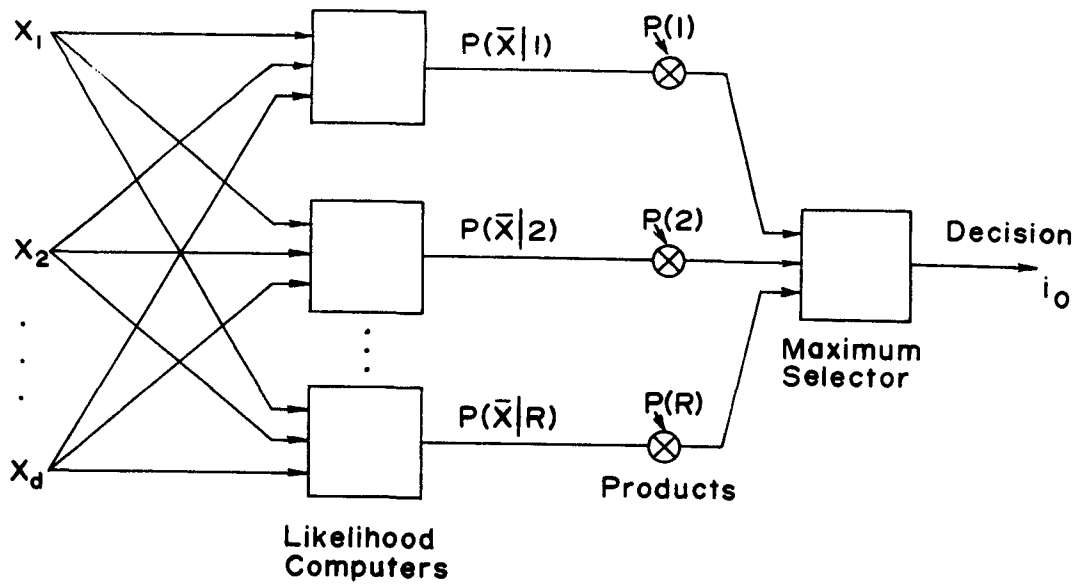


Figure 10. Bayesian Classifier

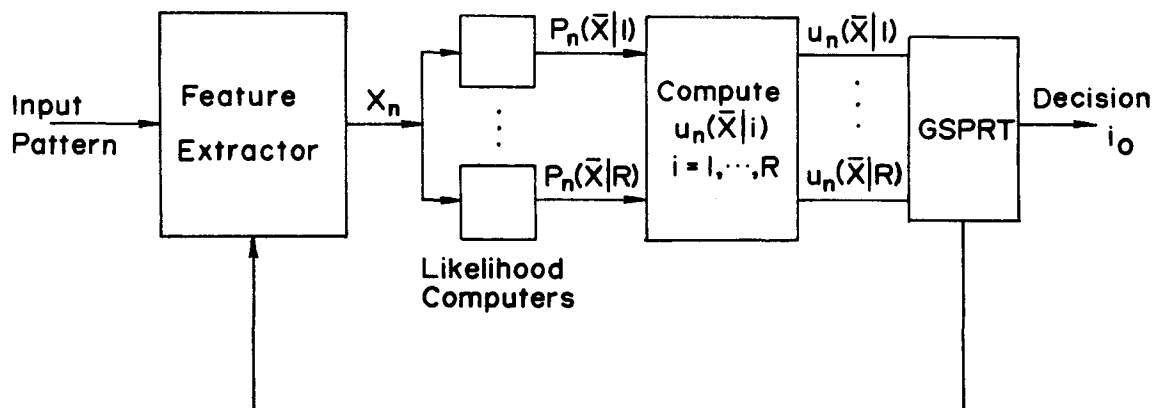


Figure 11. Sequential Classifier